Geometry and electronic structure of iridium adsorbed on graphene

Bradford A. Barker, Aaron J. Bradley, Miguel M. Ugeda, Sinisa Coh, Alex Zettl, Michael F. Crommie, Steven G. Louie, and Marvin L. Cohen

Phys. Rev. B **99**, 075431 — Published 22 February 2019

DOI: 10.1103/PhysRevB.99.075431

The Geometry and Electronic Structure of Iridium adsorbed on Graphene

Bradford A. Barker,[1,2,*] Aaron J. Bradley,[1,2] Miguel Moreno Ugeda,[3,4,5] Sinisa Coh,[6] Alex Zettl,[1,2] Michael F. Crommie,[1,2] Steven G. Louie,[1,2] and Marvin L. Cohen[1,2]

[1] *Department of Physics, University of California, Berkeley, CA 94720, USA*
[2] *Materials Sciences Division, Lawrence Berkeley National Laboratory, Berkeley, CA 94720, USA*
[3] *Donostia International Physics Center (DIPC), Manuel Lardizábal 4, 20018 San Sebastián, Spain*
[4] *Centro de Física de Materiales (CSIC-UPV/EHU), Manuel Lardizábal 5, 20018 San Sebastián, Spain*
[5] *Ikerbasque, Basque Foundation for Science, 48013 Bilbao, Spain*
[6] *Department of Mechanical Engineering, University of California, Riverside, CA 92521, USA*

(Dated: February 7, 2019)

We report investigation of the geometry and electronic structure of Iridium atoms adsorbed onto graphene through a combined experimental and theoretical study. Ir atoms were deposited onto a flake of graphene on a Pt(111) surface and found to form clusters even at low temperatures. The areal density of the observed clusters on the graphene flake suggests the clusters are most likely pairs Ir atoms. Theoretical *ab initio* density functional ("DFT") calculations indicate that these Ir dimers are oriented horizontally, near neighboring "bridge" sites of the graphene lattice, as this configuration has the strongest adsorption energy of all high-symmetry configurations for the Ir dimer. A large peak in the local density of states ("LDOS") at the Dirac point energy was measured via scanning tunneling spectroscopy, and this result is reproduced by a DFT calculation of the LDOS. The peak at the Dirac point energy is found to be from the Ir s and p states. The LDOS in the monomer case was also calculated, and is found to significantly differ from the experimentally determined data, further supporting the hypothesis of low temperature clustering.

I. INTRODUCTION

The sublattice symmetry of graphene results in a Dirac-like low-energy Hamiltonian about the K and K' points in its Brillouin Zone, which gives it the remarkable electronic properties of ultrarelativistic chiral Dirac fermions, including ballistic transport and the anomalous Integer Quantum Hall Effect[1]. Much experimental and theoretical work has been devoted to the manipulation of graphene to modify its electronic structure in novel ways[1].

A subset of these works focuses on investigating how adatoms and other adsorbates modify various electronic properties of graphene. The electronic structure of graphene with a dozen different adatoms was calculated in Ref. 2, finding slight modifications to the electronic density of states (DOS) with alkali adatoms and considerable modification to the DOS with transition metal adatoms. In particular, the linear DOS in the vicinity of the Dirac point was largely obscured by the d-like atomic states from transition metal adatoms Ti, Fe, and Pd, and the noble metal adatom Au[2].

Theoretical studies of Pd dimers adsorbed onto graphene have shown potential for hydrogen storage, as well. Pairs of hydrogen atoms prefer to dissociate and bond on opposing sides of Pd dimers instead of forming a hydrogen bond[3]. Similar results have also been reported for larger Pd clusters[4]. Further theoretical work[5–10] has focused on enhancing the weak spin-orbit coupling of graphene by using adatoms to break symmetries, as well as the intrinsic contribution of the atomic spin-orbit coupling from sufficiently heavy metallic adatoms. In particular, calculations with Au[6], W[7], Os[11], Ir[11], and In[12] adatoms suggested relatively large spin-orbit gaps with non-trivial band topologies.

Attempts at realizing these exotic electronic phases with In adatoms[13] and W adatoms[14] have shown null results, however. Initial theoretical work suggested that the adsorption of In onto the hollow site of graphene allows for a fortuitous cancellation of the Rashba spin-orbit coupling[12], thus allowing an induced quantum spin Hall effect. However, enhancement of the Coulomb scattering from the defect rendered any possible non-trivial topology unobservable. Refined first-principles scattering calculations using the quasiparticle band structure with spin-orbit coupling treated non-perturbatively[14] have supported this interpretation.

Additionally, the work with Os and Ir adatoms noted that monomers form spin moments of 0.45 μ_B and 0.30 μ_B per atom, respectively[11], breaking the time-reversal invariance required for the quantum spin Hall effect. Dimerizing the transition metal atoms with Cu was proposed to eliminate magnetic moments in the system and thus preserve time-reversal symmetry[11].

Here we show in a combined experimental and theoretical study that Ir atoms form dimers on graphene, with the electronic structure of the dimers contributing significantly to the local density of states ("LDOS") at the Dirac point energy. Section II presents the experimental work which involves using vapor deposition to adsorb Ir atoms onto graphene and then using scanning tunneling spectroscopy ("STS") measurements to characterize the resulting electronic features. Section III presents computational methods while Section IV presents density

functional calculations performed to better understand the geometry of adsorbed Ir atoms as well as their electronic structure. The theoretical results indicate that Ir dimer adsorbates bind in a horizontal configuration along carbon-carbon bond sites, in contrast with the prediction of vertical dimers binding to the hollow site in a ring of carbon atoms[11]. In Section V the results of calculations of the LDOS are shown, which suggest that $6s$ and $6p$ states from Ir atoms contribute to the peak in the LDOS at the Dirac point energy. The calculated peak in the LDOS is shown to agree well with the measured spectra.

II. EXPERIMENTAL RESULTS

All STM and STS measurements were carried out at T = 7K in an ultra-high vacuum (UHV) environment using a homebuilt scanning tunneling microscope. Graphene was grown on Pt(111) and Ir was deposited on cold samples using an Omicron e-beam evaporator. The maximum temperature of the sample during Ir evaporations ranged between 8K and 12K, with different temperatures leading to qualitatively similar coverages.

Fig. 3a shows a typical STM image of Ir clusters on bare Pt(111) and graphene/Pt(111). The graphene patch is outlined with a dotted green line. The Ir clusters appear as orange protrusions and Ir found on the graphene patch appears significantly larger than Ir on the bare Pt(111) surface. The protrusions observed on Pt(111) are identified as single Ir adatoms due to the absence of thermally-driven Ir diffusion on Pt(111) at such low temperatures[15]. Unlike on Pt(111), the size of the clusters on the graphene is not homogeneous, suggesting a varying number of atoms per cluster.

STS curves from three different Ir clusters on graphene are shown in Fig. 3b. For each of these clusters, there is a feature in the spectra that occurs at +0.33 V, which is similar in energy to the Dirac point of bare graphene on Pt(111)[16,17], as well as the onset energy of an unoccupied Pt(111) surface state[18]. The STS curves also exhibit a feature at higher energy, centered at +1.2 V.

A dI/dV map taken at a sample bias voltage of V_s = +0.33 V (the energy of the large STS feature) is shown in Fig. 3b. A majority of the clusters are seen to exhibit the spectral feature at +0.33 V.

To better understand the distribution of clusters on the surface, the atom density may be estimated from a plot of the number of clusters as a function of the area of a graphene island for a given set of calibrated deposition parameters, as shown in Fig. 3d. The black dashed line is the expected number of clusters if all were indeed single Ir atoms, equal to the density of Ir atoms on the bare Pt(111) surface. The red dashed line is the expected number of clusters if all were dimers. The majority of our data points fall closer to the dimer line, suggesting that Ir adatoms are mobile on graphene at temperatures as low as 8K and cluster with a small number of atoms to form dimers and, less frequently, trimers. The mobility of Ir adatoms on graphene may also be affected by the moiré pattern formed between graphene and Pt(111).

III. CALCULATION METHODS

The *ab initio* calculations[19] of the system were performed using the `Quantum ESPRESSO`[20] density functional theory software package. A 4×4 supercell was used for the single adatom and vertically-oriented dimer systems, and a 5 × 5 supercell is used for the horizontally-oriented dimer, with a vacuum of 15 Å in all cases, as measured from the topmost Ir atom in the system. Vanderbilt ultrasoft fully relativistic pseudopotentials[21,22] were used, along with a 40 Ry planewave kinetic energy cutoff and a 381 Ry charge density planewave cutoff. The local density approximation (LDA) was chosen for the exchange-correlation functional. In the context of graphene contacting an Ir(111) surface this gives similar results as compared to van der Waals functionals[23] (and is also consistent with Ref. 11). The metallic bonding of Ir to graphene is adequately described in the LDA, despite the systematic overestimation of binding. The Methfessel-Paxton smearing[24], appropriate for metals, has a width 0.005 Ry. The Monkhorst-Pack grid for sampling the Brillouin zone was 9×9×1 when constructing the charge density. The computational details for the DOS calculations are in Section V.

The binding energy of a single Ir adatom is calculated from $\Delta E = E_{\rm tot} - E_{\rm gr} - E_{\rm Ir}$, where $E_{\rm tot}$ is the energy of the Ir adatom-on-graphene system, $E_{\rm gr}$ is the energy of an isolated graphene supercell, and $E_{\rm Ir}$ is the energy of an isolated Ir atom. For adsorbed dimer systems, the binding energy per Ir atom is defined as $\Delta E = 1/2\,(E_{\rm tot} - E_{\rm gr} - 2E_{\rm Ir})$, with $E_{\rm tot}$ now referring to the Ir dimer-on-graphene system. The value of $E_{\rm gr}$ is scaled appropriately from the energy of a primitive graphene unit cell for the size of the supercell under consideration. Bare graphene in a primitive unit cell was relaxed, with the computed carbon-carbon distance of 1.417 Å agreeing well with the experimental value of 1.42 Å.

The Pt(111) substrate is not explicitly included in the calculations. The graphene-Pt substrate interaction will not by itself introduce a gap in the graphene Dirac cone[25], with the substrate merely introducing hybridization effects that obscure the usual linear dispersion. The dominant physical effect of the substrate is included implicitly by fixing the positions of the carbon atoms in the graphene sheet. The carbon atoms are held fixed at their independently-relaxed carbon-carbon distance of 1.417 Å when determining the relaxed coordinates of the Ir atoms. In comparing the results of the theoretical calculations to experiment, the particular values of Fermi energy differ due to the neglect of the Pt substrate, so the theoretical and experimental spectra are instead compared near the estimated Dirac point energy, E_D. This energy E_D is taken to be the zero of energy for all theo-

retical calculations.

Hopping matrix elements between Ir atoms in neighboring supercells, computed in `Wannier90`[26], were found to be at most 2 meV, indicating that the wavefunctions are well-contained in a single supercell. A small intercellular interaction was confirmed by using a 6×6 supercell calculation for the horizontally-oriented hollow-site calculation, as the adsorption energy per Ir atom changes by only 7 meV relative to the 5×5 supercell.

IV. THEORETICAL GEOMETRY

A. Single Ir adatoms

The Ir adatom is relaxed in the bridge ("B"), hollow ("H"), and top ("T") sites (shown in Fig. 1). The Ir atom favors the B site, in agreement with previous calculations using PBE and van der Waals functionals[27], in addition to calculations of single Pd adatoms.[2]. Ref. 11 finds a preference for the H site using LDA while neglecting to include corrections to the dipole interaction with periodic images in the out-of-plane direction. This result is reproduced when performing the single-atom relaxation while neglecting the correction to the dipole interaction.

Table I summarizes the binding heights h, adsorption energies ΔE, diffusion barries E_{Diff}, and magnetic moments per supercell m for the single Ir atom adsorption.

The diffusion barrier across a high-symmetry point is approximated as $E_{\mathrm{Diff}} = E_{\mathrm{a}}^{\mathrm{max}} - \Delta E$, the difference in energy from the lowest-energy geometry to the energy of the site under consideration[2]. The most appropriate approximation of the diffusion path would be one that is calculated by the nudged elastic band method to explore the full energy surface for all possible directions. However, if the diffusion is assumed most likely to occur nearly along high-symmetry directions, the barrier to diffusion along a direction is simply the difference in energy of the initial and final configurations. The estimated diffusion barriers of 0.73 eV and 0.49 eV for the top and hollow sites, respectively, are well-above room temperature and are on the order of that of Fe adsorbed on graphene[2].

The tendency for the adatoms on graphene to form clusters can be estimated by comparing the binding energy per atom ΔE to the bulk cohesive energy per atom E_{c}. A ratio of $\Delta E/E_{\mathrm{c}} \sim 1$ indicates a strong adsorption energy of the adatom and therefore a tendency to bind to graphene as an adatom; the limit $\Delta E/E_{\mathrm{c}} << 1$ indicates a tendency to cluster[2]. However, the LDA overestimates cohesive energies for solids, particularly $5d$ transition metals[28], so the experimental value of $E_{\mathrm{c}} = 6.94$ eV[28] is used instead. With the adsorption energy at the bridge site $\Delta E = 1.86$ eV, the ratio is 0.268. Though this ratio may still be overestimated due to the use of the LDA for the calculation of the binding energy, this result may be compared to the value of 0.307 reported for Al[2], which is also known experimentally to form clusters with three atoms when adsorbed to graphite[29,30]. This estimation suggests that Ir tends to cluster on graphene, which is supported by experiment (Fig. 3d).

B. Ir Dimers

The horizontal dimer at the bridge sites B^1 and B^2 (see Fig. 1) has the largest adsorption energy for any of the considered dimer configurations, horizontal or vertical, and so it is the most likely orientation for the observed two-atom clusters at low temperature (the individual atoms within a dimer could not be resolve via STM). The bonding distances for the horizontal dimers (2.32-2.46 Å) are longer than in isolation, 2.23 Å[31], and are on the order of the next-nearest-neighbor C-C bond length, 2.46 Å. Indeed, the bridge-site dimer has the shortest Ir-Ir distance, explaining its favorable adsorption energy, as it is stretched from its value in isolation the least. By comparing the adsorption energy per atom for this dimer (Table II) and the single adatom (Table I), it is found that each Ir atom favors the formation of a dimer by 1.5 eV.

The estimated diffusion barrier is computed for the dimer as a whole, defined by $E_{\mathrm{Diff}} = 2\,(E_{\mathrm{a}}^{\mathrm{max}} - \Delta E)$. The hollow site has an estimated diffusion barrier of 1.02 eV, indicating a stronger preference to diffuse through the top site, with much lower estimated diffusion barrier of 0.34 eV, which may allow a pathway to form larger clusters. The magnetic moment per unit-cell is consequently increased to over 1 μ_{B} per Ir atom. The magnetic moment now has a large in-plane component in addition to the out-of-plane component, due to the in-plane dimer bond defining an additional axis for the magnetic moment.

The binding energies per Ir atom in the vertical dimer configuration are nearly identical for the B, H, and T positions, with 3.11 eV for B and T, and 3.14 eV for H, giving small diffusion barriers of 0.06 eV, comparable to room temperature. The distance from the bottom-most Ir atom in the dimer to the graphene sheet (h_b in Table III and Fig. 2) is larger than for the single Ir adatom case.

V. ELECTRONIC STRUCTURE

A. Single Ir adatoms

The DOS of pristine graphene in a primitive unit cell is calculated with a 96×96×1 Monkhorst-Pack grid, which is dense enough to resolve the zero DOS at the Dirac point energy. An adsorbate atop a 4×4 supercell of graphene needs only a 24×24×1 grid to give an overall sampling density equivalent to that of pristine graphene for DOS calculations. Fig. 4 shows a comparison of of the Ir monomer adsorbate DOS compared to the bare

graphene DOS. The peaks in the adsorbate DOS arising from the weakly-hybridized, low-lying sp^2 states may be matched with that of pristine graphene (Fig. 4) to provide an estimate to the Dirac point.

For comparison with the experimental STS spectra, the LDOS is calculated 4 Å above the Ir atoms. The delta functions in the LDOS are taken to be Gaussian functions with a smearing of 75 meV. The resulting LDOS (Fig. 5) shows a significant peak about 0.5 eV above the Dirac point energy, with a much weaker peak at the Dirac point energy and other peaks further away in energy. This does not match the experimental dI/dV spectra and suggests that the experimentally observed peaks (Fig. 3c) do not come from this configuration of single adatoms. By comparing the single Ir adatom LDOS with the partial density of states ("PDOS"), which resolves the contributions the Ir s, p, and d states make to the DOS, the Ir s- and p-states are found to give the most significant contribution to the large peak, with the d-states being localized below the 4 Å simulated tip placement (Fig. 6).

B. Ir Dimers

The DOS, LDOS, and PDOS for the adsorbed dimer system were similarly computed. As with the Ir monomer, the Ir dimer DOS (Fig. 7) shows that the low-lying sp^2 states from graphene are only weakly hybridized with the Ir states and therefore allow for an estimation of the Dirac point energy. The calculated Ir LDOS shows a large peak near the estimated Dirac point energy (Fig. 8), as observed in experiment. This suggests that the Ir clusters are indeed a pair of B-site Ir adatoms in the horizontal dimer configuration. The PDOS (Fig. 9) shows a significant contribution from the Ir 5d states. However, a comparison of the LDOS with PDOS (Fig. 10) shows that the features of the LDOS (especially within a 1 eV window about the Dirac point energy) appear to arise from the sum of the 6s- and 6p-states, since these states have a longer spatial extent than the 5d states.

Fig. 11 directly compares the measured $\mathrm{d}I/\mathrm{d}V$ spectrum of an Ir/graphene cluster with the calculated dimer LDOS, plotted in arbitrary units such that both curves are matched at the central peak height. There is good agreement with the placement of the central peak. The higher-energy feature seen experimentally also seems to be reproduced, though within a significantly red-shifted energy range, likely due to DFT underestimation of excited-state energies. The peaks below the estimated Dirac point energy that are present in the calculated LDOS are suppressed in the measured spectrum.

VI. CONCLUSION

Ir atoms deposited on graphene/Pt(111) are experimentally found to form clusters, even at low temperatures. By calculating the areal density of the observed clusters on the graphene flake, the typical size of the clusters are estimated to be composed of two Ir atoms. This matches the results of *ab initio* calculations. Our simulations suggest that Ir dimers are oriented horizontally at the bridge sites of the graphene lattice. The peaks in the experimental and theoretical LDOS near the Dirac point energy match well and may be attributed to the Ir dimer 6s and 6p states. The LDOS for a single adatom is found to have significantly different peak locations and amplitudes than that of experiment, further supporting the conclusion that the experimentally observed Ir structures are dimers.

VII. ACKNOWLEDGMENTS

The authors would like to thank Sehoon Oh and Ting Cao for useful discussions. This work was supported by the Director, Office of Science, Office of Basic Energy Sciences, Materials Sciences and Engineering Division, of the U.S. Department of Energy under Contract No. DE-AC02-05-CH11231, within the sp2-Bonded Materials Program (KC2207), (DFT simulated electronic structure and STM spectroscopy). Support was also provided by National Science Foundation grants DMR-1508412 (diffusivity analysis) and DMR-1807233 (sample preparation). Computational resources have been provided by the DOE at Lawrence Berkeley National Laboratory's NERSC facility.

* bbarker@berkeley.edu

[1] A. H. Castro Neto, F. Guinea, N. M. R. Peres, K. S. Novoselov, and A. K. Geim, Rev. Mod. Phys. **81**, 109 (2009).
[2] K. T. Chan, J. B. Neaton, and M. L. Cohen, Phys. Rev. B **77**, 235430 (2008).
[3] I. Lopez-Corral, E. Germán, A. Juan, M. Volpe, and G. Brizuela, international journal of hydrogen energy **37**, 6653 (2012).
[4] I. Cabria, M. López, S. Fraile, and J. Alonso, The Journal of Physical Chemistry C **116**, 21179 (2012).
[5] A. H. Castro Neto and F. Guinea, Phys. Rev. Lett. **103**, 026804 (2009).
[6] D. Ma, Z. Li, and Z. Yang, Carbon **50**, 297 (2012).
[7] H. Zhang, C. Lazo, S. Blügel, S. Heinze, and Y. Mokrousov, Phys. Rev. Lett. **108**, 056802 (2012).
[8] Y. Li, P. Tang, P. Chen, J. Wu, B.-L. Gu, Y. Fang, S. B. Zhang, and W. Duan, Phys. Rev. B **87**, 245127 (2013).
[9] J. Ding, Z. Qiao, W. Feng, Y. Yao, and Q. Niu, Phys. Rev. B **84**, 195444 (2011).
[10] Z. Qiao, S. A. Yang, W. Feng, W.-K. Tse, J. Ding, Y. Yao, J. Wang, and Q. Niu, Phys. Rev. B **82**, 161414 (2010).

[11] J. Hu, J. Alicea, R. Wu, and M. Franz, Phys. Rev. Lett. **109**, 266801 (2012).
[12] C. Weeks, J. Hu, J. Alicea, M. Franz, and R. Wu, Phys. Rev. X **1**, 021001 (2011).
[13] Z. Jia, B. Yan, J. Niu, Q. Han, R. Zhu, D. Yu, and X. Wu, Phys. Rev. B **91**, 085411 (2015).
[14] F. J. d. Santos, D. A. Bahamon, R. B. Muniz, K. McKenna, E. V. Castro, J. Lischner, and A. Ferreira, arXiv:1712.07827 (2017).
[15] D. Bassett and P. Webber, Surface Science **70**, 520 (1978).
[16] P. Sutter, J. T. Sadowski, and E. Sutter, Phys. Rev. B **80**, 245411 (2009).
[17] M. M. Ugeda, D. Fernández-Torre, I. Brihuega, P. Pou, A. J. Martínez-Galera, R. Pérez, and J. M. Gómez-Rodríguez, Phys. Rev. Lett. **107**, 116803 (2011).
[18] J. Wiebe, F. Meier, K. Hashimoto, G. Bihlmayer, S. Blügel, P. Ferriani, S. Heinze, and R. Wiesendanger, Phys. Rev. B **72**, 193406 (2005).
[19] M. L. Cohen, M. Schlüter, J. R. Chelikowsky, and S. G. Louie, Phys. Rev. B **12**, 5575 (1975).
[20] P. Giannozzi, S. Baroni, N. Bonini, M. Calandra, R. Car, C. Cavazzoni, D. Ceresoli, G. L. Chiarotti, M. Cococcioni, I. Dabo, A. D. Corso, S. de Gironcoli, S. Fabris, G. Fratesi, R. Gebauer, U. Gerstmann, C. Gougoussis, A. Kokalj, M. Lazzeri, L. Martin-Samos, N. Marzari, F. Mauri, R. Mazzarello, S. Paolini, A. Pasquarello, L. Paulatto, C. Sbraccia, S. Scandolo, G. Sclauzero, A. P. Seitsonen, A. Smogunov, P. Umari, and R. M. Wentzcovitch, Journal of Physics: Condensed Matter **21**, 395502 (2009).
[21] D. Vanderbilt, Phys. Rev. B **41**, 7892 (1990).
[22] A. Dal Corso, Computational Materials Science **95**, 337 (2014).
[23] R. Brako, D. Šokčević, P. Lazić, and N. Atodiresei, New Journal of Physics **12**, 113016 (2010).
[24] M. Methfessel and A. T. Paxton, Phys. Rev. B **40**, 3616 (1989).
[25] Q. Zhou, S. Coh, M. L. Cohen, S. G. Louie, and A. Zettl, Phys. Rev. B **88**, 235431 (2013).
[26] A. A. Mostofi, J. R. Yates, Y.-S. Lee, I. Souza, D. Vanderbilt, and N. Marzari, Computer Physics Communications **178**, 685 (2008).
[27] I. A. Pašti, A. Jovanović, A. S. Dobrota, S. V. Mentus, B. Johansson, and N. V. Skorodumova, arXiv:1710.08985 (2017).
[28] R. E. Watson, G. W. Fernando, M. Weinert, Y. J. Wang, and J. W. Davenport, Phys. Rev. B **43**, 1455 (1991).
[29] E. Ganz, K. Sattler, and J. Clarke, Surface Science **219**, 33 (1989).
[30] V. Maurice and P. Marcus, Surface Science **275**, 65 (1992).
[31] J. L. Jules and J. R. Lombardi, The Journal of Physical Chemistry A **107**, 1268 (2003).

TABLE I: Calculated values of the height, h, the binding energy, ΔE, the diffusion barrier, $E_{\rm Diff}$, and the magnetic moment per supercell, m for single Ir atoms bound to the bridge, hollow, and top configurations.

Config.	h (Å)	ΔE (eV)	$E_{\rm Diff}$ (eV)	m ($\mu_{\rm B}$)
Bridge	1.95	1.86	–	0.95
Hollow	1.70	1.13	0.73	0.61
Top	1.93	1.37	0.49	0.99

TABLE II: Calculated values of the relaxed height of each Ir atom, h, the inter-Ir distance, $d_{\rm Ir\text{-}Ir}$, the adsorption energy, ΔE, the diffusion barrier, $E_{\rm Diff}$, and the projected components of the magnetic moment per supercell, $m_{x,y,z}$, for horizontally oriented Ir dimers bound to the B/H/T 1 and B/H/T 2 sites of graphene.

Config.	$h_{1=2}$ (Å)	$d_{\rm Ir\text{-}Ir}$ (Å)	ΔE (eV)	$E_{\rm Diff}$ (eV)	m_x ($\mu_{\rm B}$)	m_y ($\mu_{\rm B}$)	m_z ($\mu_{\rm B}$)
$B^1 - B^2$	2.05	2.32	3.36	–	0.00	1.06	1.29
$H^1 - H^2$	1.88	2.46	2.85	1.02	0.00	0.00	1.32
$T^1 - T^2$	2.10	2.45	3.19	0.34	0.23	0.23	1.28

TABLE III: Calculated values of the relaxed height of each Ir atom, h, the inter-Ir distance, $d_{\rm Ir\text{-}Ir}$, the adsorption energy, ΔE, the diffusion barrier, $E_{\rm Diff}$, the out-of-plane magnetic moments for each Ir atom, $m_{b,t}$, and the magnetic moment per supercell, m, for vertically oriented Ir dimers in the hollow, bridge, and top configurations.

Config.	h_b (Å)	$d_{\rm Ir\text{-}Ir}$ (Å)	ΔE (eV)	$E_{\rm Diff}$ (eV)	m_b ($\mu_{\rm B}$)	m_t ($\mu_{\rm B}$)	m ($\mu_{\rm B}$)
Bridge	2.41	2.19	3.11	0.06	0.58	0.67	2.07
Hollow	2.29	2.19	3.14	–	0.54	0.77	2.00
Top	2.40	2.18	3.11	0.06	0.58	0.68	2.05

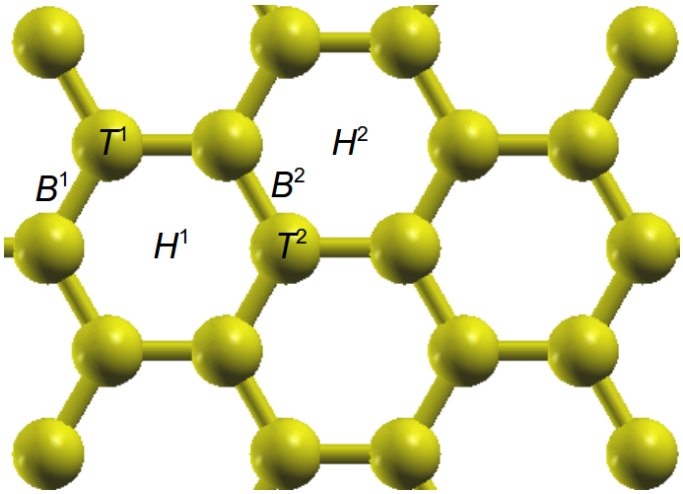

FIG. 1: Sketch of different adsorption sites: bridge (B^1, B^2), hollow (H^1, H^2), and top (T^1, T^2). In the monomer and vertical dimer cases, only B^1, H^1, and T^1 are considered and are referred to as B, H, and T, respectively.

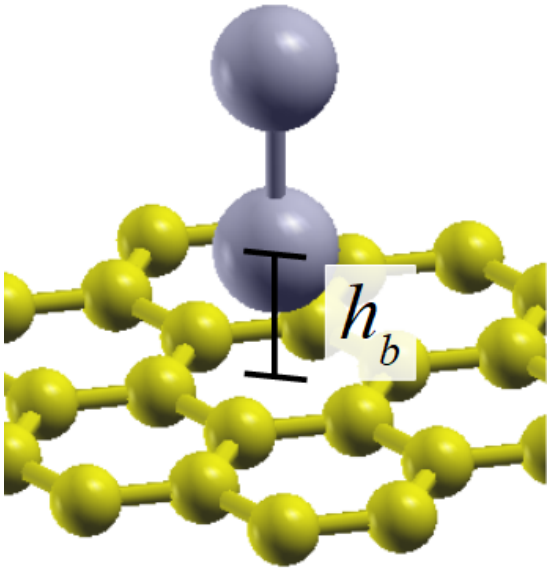

FIG. 2: Vertical configuration of the Ir dimer over the hollow site. The distance of the bottom-most Ir atom to the graphene plane is h_b.

(a)

(b)

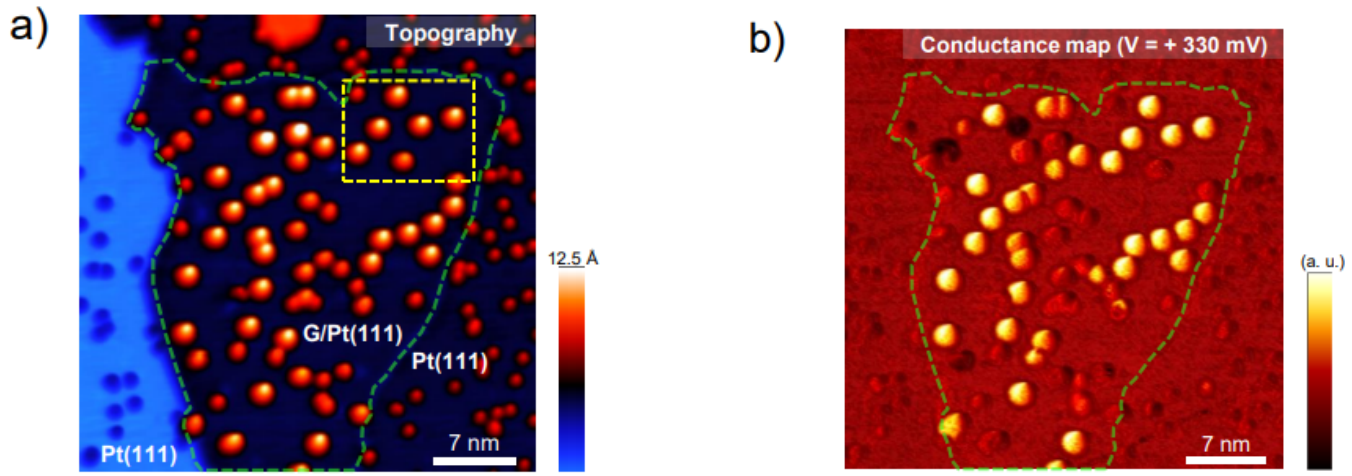

(c)

(d)

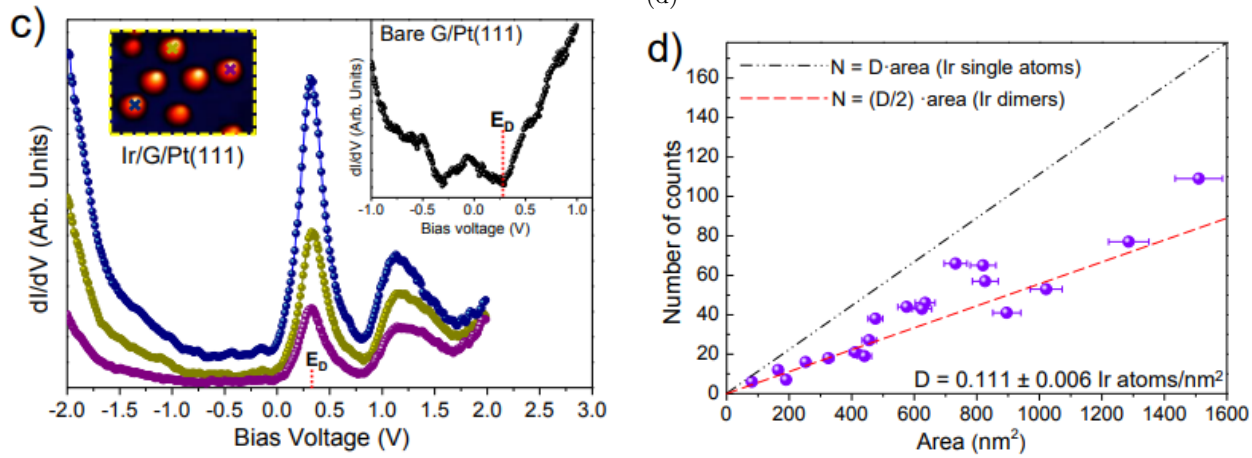

FIG. 3: (a): STM topography of Ir clusters on bare Pt(111) and graphene/Pt(111). The graphene flake is within the green dashed contour, and the Ir clusters under consideration are within the yellow dotted rectangle ($V_s = 0.33$V, $I = 1$nA). (b): The dI/dV map of the same region acquired simultaneously with (a). (c): dI/dV spectra for the Ir clusters indicated in the top-left inset. The top-right inset is the dI/dV spectrum for the bare graphene flake away from the Ir clusters (dI/dV parameters: $V_{rms} = 4$ mV, wiggle freq. = 2140 Hz, initial $I = 1$nA). The estimated Dirac point is indicated by the vertical dashed red line. (d): The number of clusters as a function of the area of the graphene island. The black dash-dotted line has a slope with a density corresponding to one Ir atom per cluster. The red dashed line corresponds to two Ir atoms per cluster.

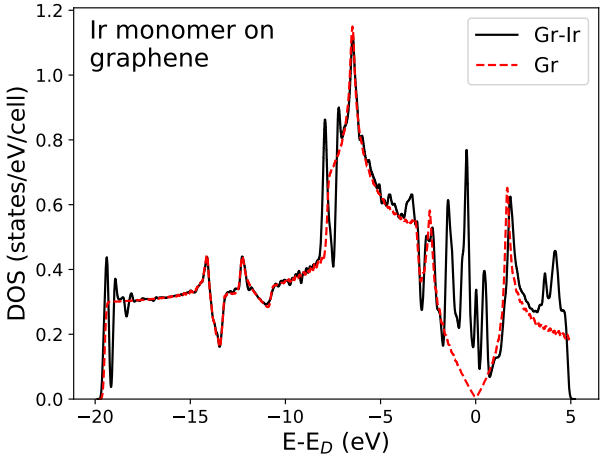

FIG. 4: Comparison between the calculated DOS for pristine graphene and for a single Ir adatom on graphene, in a 4x4 supercell. The DOS for the supercell is averaged over the primitive cells.

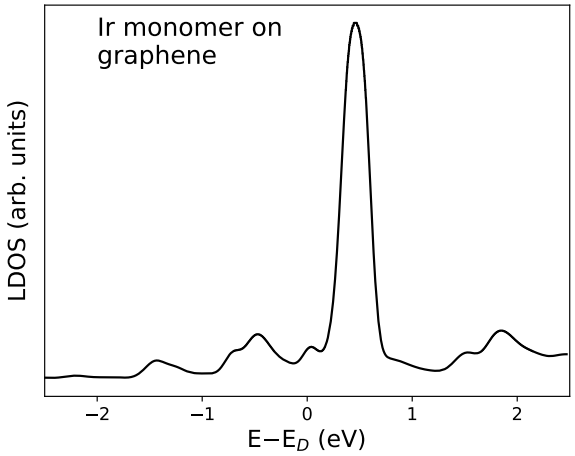

FIG. 5: The calculated LDOS for a single Ir adatom on graphene, calculated 4 Å above the Ir atom.

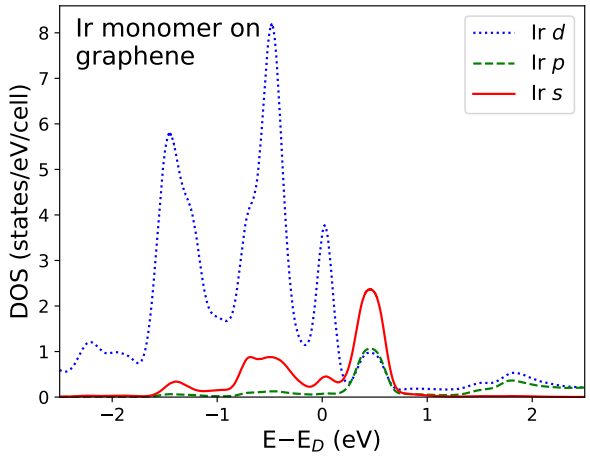

FIG. 6: The calculated PDOS for a single Ir adatom on graphene at energies relative to the Dirac point energy.

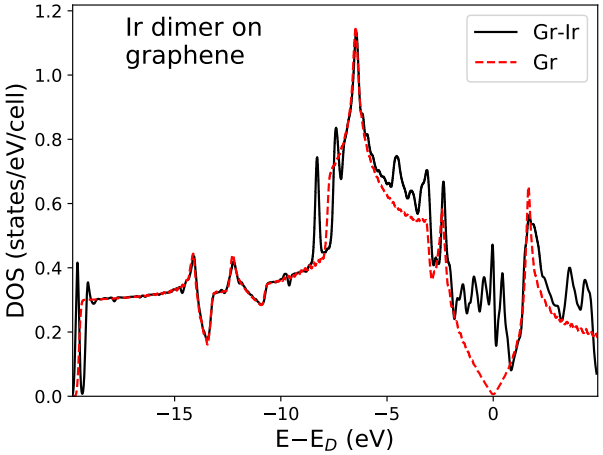

FIG. 7: Comparison of the calculated DOS for a pristine sheet of graphene and an Ir dimer adsorbed onto graphene, in a 5x5 supercell. The DOS for the supercell is averaged over the primitive cells.

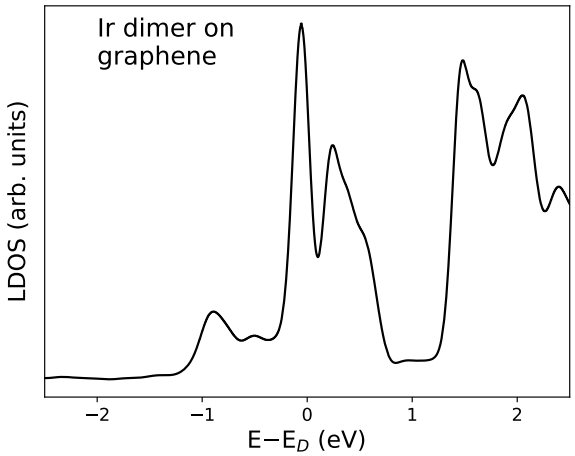

FIG. 8: The calculated LDOS 4 Å above an Ir dimer on graphene at energies relative to the Dirac point energy.

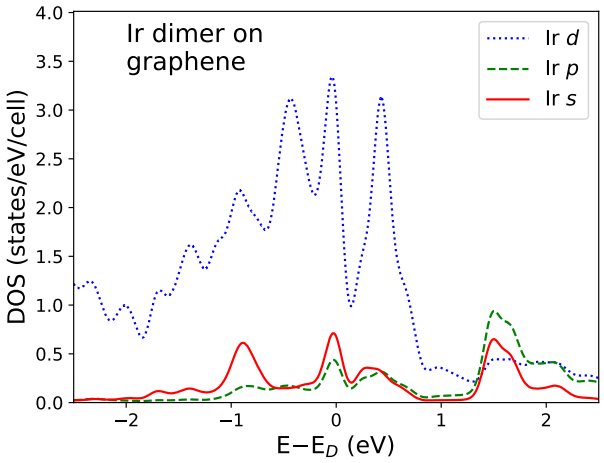

FIG. 9: The calculated PDOS for an Ir dimer on graphene at energies relative to the Dirac point energy.

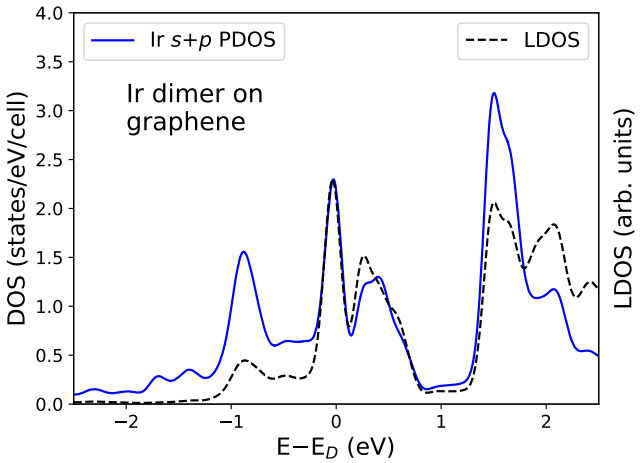

FIG. 10: The calculated PDOS from the sum of Ir 6s and 6p orbitals, compared to the total LDOS for an Ir dimer on graphene at energies relative to the Dirac point energy. The curves are normalized so that the central peaks of the LDOS and PDOS have equal heights.

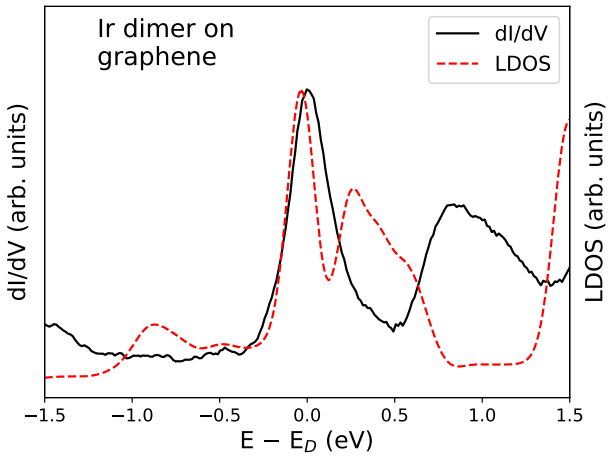

FIG. 11: Comparison of experimentally determined dI/dV for an Ir cluster on graphene/Pt(111) (solid black curve) and calculated LDOS for an Ir dimer on graphene (dashed red curve) at energies relative to the Dirac point energy.